Preparation and Ground-State Electronic Structure of Heterobimetallic Yb–Pt IV -Alkyl Complexes

Maxime Tricoire, Grégory Danoun, Grégory Nocton

Preparation and Ground-state Electronic Structure of Heterobimetallic Yb-Pt^{IV}-alkyl complexes

Maxime Tricoire, Grégory Danoun* and Grégory Nocton*

LCM, CNRS, Ecole polytechnique, Institut polytechnique de Paris, Route de Saclay, 91120 Palaiseau, France. E-mail: gregory.danoun@polytechnique.edu; gregory.nocton@polytechnique.edu

Abstract

This article focuses on the synthesis of heterobimetallic complexes of lanthanide and platinum. It describes the synthesis of the Cp*Yb(bipym)$PtMe_2$ complex and its characterization, followed by its reactivity with oxidants, giving access to various Pt +IV compounds of trismethyl ($PtMe_3$) and tetramethyl ($PtMe_4$) fragments. Characterization of the electronic properties of the complexes by magnetic measurements demonstrated that the tetramethyl complex possesses a singlet ground state. The trismethyl fragments, on the other hand, have a ground state that evolves as a function of the ligand saturating the coordination sphere: singlet for triflate and pyridine and triplet for iodine, demonstrating the capacity for simple tuning of the electronic structure of these complexes. While the addition of $B(C_6F_5)_3$ to the platinum +II bis methyl complex leads to FLP-like reactivity triggering THF opening, reactivity with $[Ph_3C]^+[BPh_4]^-$ leads to oxidation of the bipym ligand. Furthermore, the light reactivity of the tetramethyl complex indicated the possible transfer of a methyl group, leading to the functionalization of the bridging bipym ligand.

Introduction

The control of the electronic ground – and close excited states of metal complexes is relevant for the development of chemical objects with specific magnetic or optical properties but also in the preparation of tailored catalysts with good control of the chemical selectivity.[1–3] To do so, the modulation of the HOMO-LUMO gap is achieved through adapted ligand design and meticulous metal choice to obtain the desired outcome, such as light-induced reactions,[4,5] controlled spin-crossover processes,[6,7] or even two-state reactivity.[8–10] In recent years, a growing interest has been shown in metal cooperativity in multimetallic systems, especially in heterometallic architectures, where the metal centers benefit from synergetic efforts.[11–13] Among the possible assemblies, the combinations of a 4-f ion and a d-metal are somewhat limited to trivalent lanthanide precursors and have been rarely investigated for reactivity.[14–18]

Due to the population of their 4-f shell, the intrinsic electronic properties of lanthanides are substantially different than the ones of transition metals.[19] This has resulted in singular structural features and spectroscopic signatures.[20–26] These studies contributed to the development of many experimental and theoretical methodologies,[27–30] ultimately leading to the concept of intermediate valence in lanthanide complexes.[31] Seminal studies on divalent ytterbium complexes and N-heterocycle metal-ligand pairs, $Cp^*_2Yb(L)$, allowed tuning the electronic structures by adapting the relative energy and the symmetry of the molecular orbital of the fragment, leading to different reactivity outcomes.[27,28,32–35] The concept was thus extended with transition metal complexes of aromatic *N*-heterocyclic ligands as the L fragment.

As such, the combination of a divalent lanthanide with a redox-active metal complex of group 10 has been previously reported with Pd and Ni in various oxidation states. Notably, the nature of the ground state, triplet vs. singlet, has been shown to induce substantial modifications when the bridging ligand was modified from the symmetrical 2,2'-bipyrimidine (bipym), to the 4,5,9,10-tetraazaphenantrene (taphen), or to the unsymmetrical 2-pyrimidin-2-yl-benzimidazole (bimpm) ligands.[36–40] Aside from the nature of the bridging ligand, an essential question that remained was how the transition metal oxidation state exerted an influence on the nature of the ground state. This question was previously discussed with reactive Pd and Ni species in high – or low,[36,41] oxidation states but was rendered elusive because of significantly fast reactivity, yielding, at best, to intermediates. Thus, we decided to extend our previous work to Pt complexes, which featured more stable redox states over the 0 to +IV range (Figure 1).

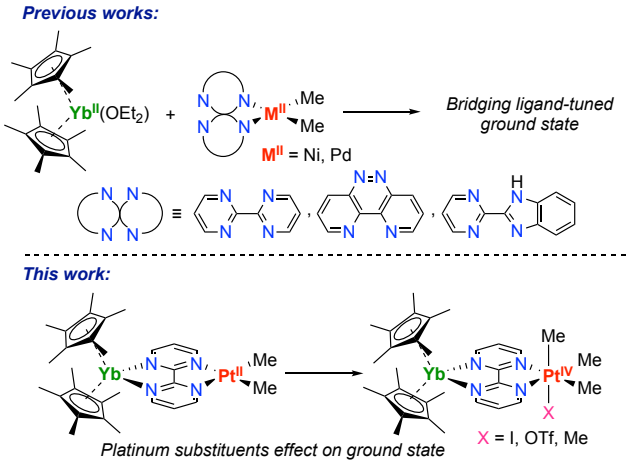

Figure 1. Ground state investigations of heterobimetallic ytterbium-group 10 metals complexes

After the seminal works of Shilov and coworkers,[42,43] who reported the C-H activation of inert alkanes by a Pt complex, platinum alkyl chemistry has been significantly focused on the understanding and the improvement of this catalytic conversion of methane.[44] Among other aspects, the nature of the C-H activation was thoroughly studied, and both the oxidative addition of a C-H bond and the electrophilic activation of a σ-bonded CH_4 molecule paths were found to be in equilibrium.[45,46] Although the Shilov system was a paramount breakthrough in the field, it still suffered from a significant drawback as it required stoichiometric amounts of platinum. This issue was later solved by Periana and co-workers with the now-known catalytic system, where the (bypm)$PtCl_2$ complex was combined with hot H_2SO_4 to convert methane to methyl bisulfate.[47] In this system, the role of the bipym ligand was significantly highlighted because its protonation to bipymH$^+$ or bipymH$_2^{2+}$ in such a strongly acidic environment was found to both lower the C-H activation energy barrier and stabilize the intermediates of the cycle.[48–50] The importance of bidentate N-heteroaromatic ligands in high-valent Pt systems was also supported mainly by the works of Puddephatt and co-workers and allowed to observe original reactivities and characterize many Pt^{IV} species to serve as a model for their high-valent palladium compounds that remain challenging to be isolated.[51–53]

Following the methodology developed for the synthesis of heterobimetallic Cp*$_2$Yb(bipym)MMe$_2$ complexes (M = Ni, Pd), we now report the isolation of their Pt analog and its reactivity studies. The intrinsic higher thermal stability of high-valent Pt species allowed the preparation of a series of several heterobimetallic complexes containing a Pt^{IV} center. The magnetic characterization of these species containing high-valent Pt centers unveiled the possibility of tuning its reactivity by modulating the singlet-triplet energy gap in those systems, a strategy that may trigger state-selective reactivity due to the tuned electronics of the bipym ligand.

Results and Discussion

Synthesis and structural analysis

The synthesis of the (bipym)$PtMe_2$ precursor, 1, was already reported and was performed in CH_2Cl_2 starting from the $[Pt(SMe_2)Me_2]_2$ dimeric precursor.[54–57] Excess of the bipym ligand was used to limit the formation of the undesired Me_2Pt(bipym)$PtMe_2$ dimer, and a crystallization step was necessary to remove the remaining free ligand. As specified in previous work with a similar complex of the same metal group,[36,37] any free ligand contamination of **1** resulted in the formation of the undesired Cp^*_2Yb(bipym)$YbCp^*_2$ dimer upon addition of the $Cp^*_2Yb(OEt_2)$ complex.[58] With this purity prerequisite, the Cp^*_2Yb(bipym)$PtMe_2$, **2**, complex was synthesized in toluene using a similar protocol as used in previous published work (Figure 2).[36,37] After the room temperature addition of a toluene solution of $Cp^*_2Yb(OEt_2)$ to a toluene suspension of 1, 2 was isolated as deep dark green X-ray suitable crystals in 86% yield after storing the solution overnight at -40 °C. The comparison of **1** and **2** XRD structures allowed us to observe that the divalent Yb transferred an electron to the bipym ligand (Figure 3 and Table 1). A typical diagnostic distance for the reduction of the ligand is the C-C bond bridging the two pyrimidine rings.[36,37,59,60] In **2**, the distance was shortened by almost 0.1 Å, 1.49(2) Å in 1 vs 1.408(5) Å in **2**. This is in agreement with a formal ligand reduction because of the transfer of one electron to the b_1 LUMO of 1 (C_{2v} symmetry), in which most of the electronic density was found on this bridging C-C bond. The b_1 orbital has a high spin density localized on the carbons connecting the two pyrimidines. As a result, its population by the additional electron favors the bonding character C-C bond, and its bonding index increases from a single bond to a formal double bond. Another metric parameter, which is of interest in this regard is the Yb-Cp^*_{Ctr} distance. The 2.31(1) Å found in 2 was coherent with a formal Yb^{III} oxidation state,[61] and thus of a formal oxidation of the ytterbium center upon coordination to the bipym ligand. In the Pt coordination environment, no significant change was noticed in the Pt-N distances of 2.09(2) Å for 1 and 2.088(4) Å for 2, while Pt-Me distances were 2.05(3) Å in 1 and 2.037(9) Å in **2**, respectively.

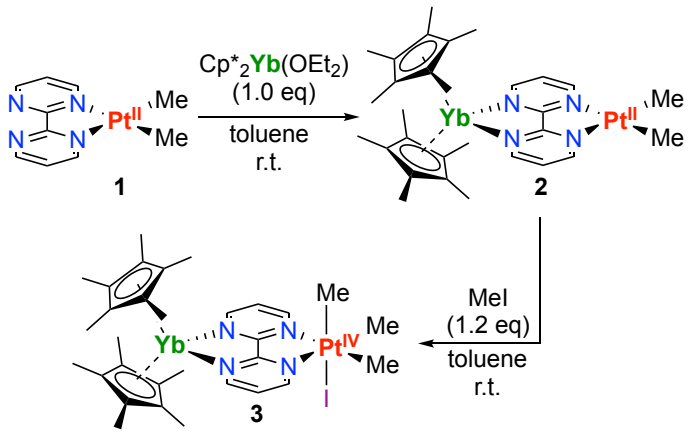

Figure 2. Synthesis of complexes Cp^*_2Yb(bipym)$PtMe_2$, **2** and Cp^*_2Yb(bipym)$PtMe_3I$, **3**.

Upon addition of MeI to a toluene solution of **2**, the coloration of the solution turned brown, and X-ray suitable needles were grown overnight at – 40 °C in 92% yield. The XRD study of these crystals obtained from toluene was not straightforward. At 150 K, images indicative of several twins were recorded. This was thought to be due to toluene cavities, and decent data was only obtained at 280 K, revealing that the oxidative addition of MeI led to the $Cp^*_2Yb(bipym)PtMe_3I$ complex, **3**, in which the C_2 axis left place to a mirror plane leading to a C_s symmetry. The resulting distances on the Pt center were slightly modified compared to 2, and the Pt-Me average distance was 2.06(4) Å while the Pt-N distance was 2.15(1) Å. Those values were within the standard range for a Pt^{IV} ion.[62–64]

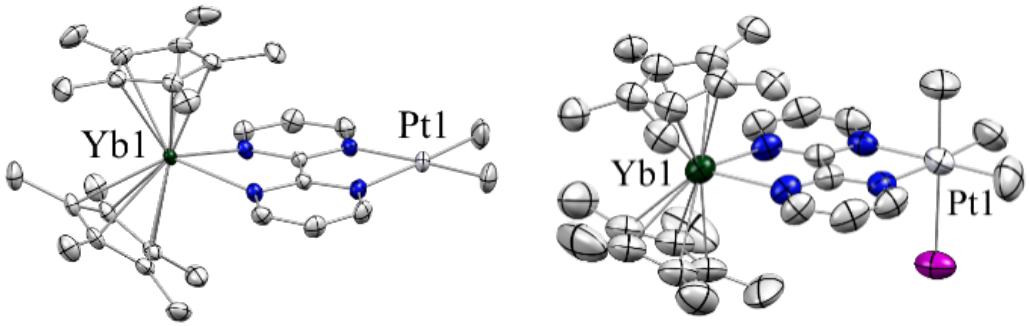

Figure 3. ORTEPs of complexes **2** (left) and 3 (right) with thermal ellipsoids at 50 % level. Carbon atoms are in grey, nitrogen atoms in blue, the iodide atom in purple, the platinum atom in white, and the ytterbium atom in olive green. Hydrogen atoms and co-crystallized toluene molecules have been removed for clarity.

Experimental electronic structure studies.

In the ^{1}H NMR spectrum of **2**, recorded at 20 °C in tol-d_8, a Cp* signal integrated for 30 hydrogen atoms was found at 5.88 ppm, two signals of the bipym ligand were highly shifted at 255.46 and -166.89 ppm, while the third was located at 6.39 ppm. The single signal corresponding to the two methyl groups was found at 17.89 ppm (Figure S1). This situation agreed with the C_{2v} symmetry observed in the solid state. The large isotropic chemical shift of two signals of the bipym ligand was consistent with the paramagnetic nature of **2**. This would not be the case with a divalent Yb^{II} (f^{14}) ion. The solution-state NMR was, therefore, in agreement with the solid-state XRD analysis; the Yb was formally oxidized (f^{13}), and the bipym ligand was better described as a radical anion. The ^{1}H NMR spectrum of **3** recorded in thf-d_8 presented a similar paramagnetic behavior to the one observed with **2**. However, since the C_{2v} symmetry was lowered to C_s after the oxidative addition, the Cp* signal was split into two resonances, found at 6.29 ppm and 6.42 ppm. The chemical shifts of the bipym signals were also slightly shifted compared to **2** with resonances at 266.71, -187.49, and 13.10 ppm, respectively. The two equatorial Me groups were found at -0.43 ppm and the axial at -13.56 ppm (Figure S3). Contrary to its Pd analog,[36] **3** was found stable at room temperature regarding reductive elimination in both the solid-state and in solution.

Further investigations were performed to probe the electronic ground state of **2** and **3**. The paramagnetic character of both compounds implicated an electron transfer from the divalent ytterbium to the bridging ligand, and yet either the formation of a triplet ground state (S = 1) or in a singlet ground state (S = 0) with a room temperature populated low-lying triplet (Figure 4). A variable temperature (VT) NMR study was performed. All the chemical shifts of **2** and **3** were plotted versus 1/T (Figures S2 and S4). As was already observed in similar systems, the plots showed a deviation from the Curie-Weiss law.[28,36,37,61,65] This was symptomatic of the magnetic exchange coupling between the two single electrons but still not answering the question about the ground state of the two complexes.

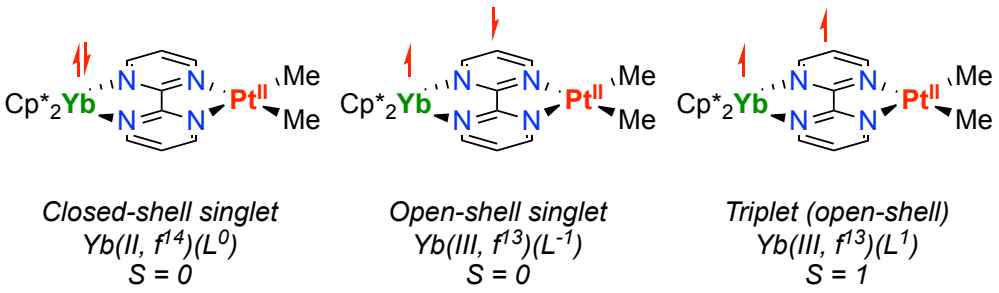

Figure 4. Different possible electronic configurations of **2**.

Solid-state magnetic studies were conducted to study the species on a larger temperature range, between 2 and 300 K. The χT versus T plot recorded under a 0.5 T field showed a χT value going toward 0 at lower temperature, in agreement with the ground state of 2 being a singlet. With the increasing temperature, the χT value increased to a room temperature value of 2.44 cm^3 K mol^{-1} (Figure 5). This value was close to the expected value for an isolated $^2F_{7/2}$ Yb^{III} paramagnet 2.57 cm^3 K mol^{-1} at 300 K.[61] This was the consequence of the triplet state being gradually populated upon the temperature increase. While Ni and Pd analogs were found to behave similarly, in this precise case, it could also be observed upon freezing a dark brown-green solution of **2** in liquid nitrogen. The triplet state was then only marginally populated, and the frozen solution turned orange.

By plotting χ versus T, several additional observations were obtained. At low temperatures, a temperature-independent paramagnetism (TIP) or Van Vleck paramagnetism was observed,[66] such behavior was caused by the small energy gap between the ground state and the low-lying excited state. The susceptibility rose to reach a maximum of around 130 K before decreasing as the temperature continued to increase. Since the susceptibility value during the TIP regime χ_{TIP} was caused by the small singlet-triplet energy gap, its incorporation in a modified Bleaney-Bowers equation permitted an estimation of the energy gap (Figure 5 and Equation S1).[67] Considering the χ_{TIP} value of 0.0073 cm^3 mol^{-1}, the χ plot versus T is fitted with a g_{ave} value of 3.68, which was relatively close to similar systems: 3.315 for instance for the $Cp^*_2Yb(bipy)^+$ cation.[68]

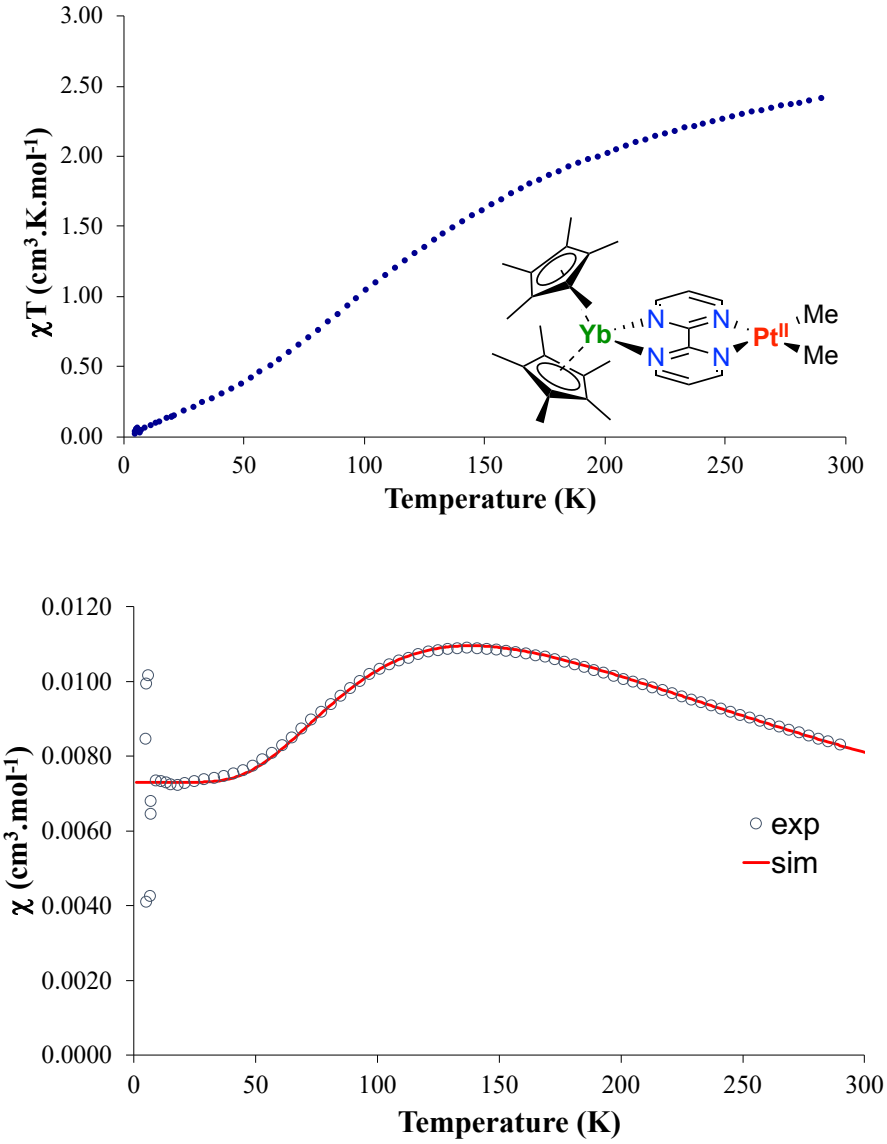

Figure 5. Solid-state temperature-dependent magnetic data of complex **2** recorded at 0.5 T: (top) χT vs T plot and (bottom) χ vs T plot and its simulation with the TIP-including Bleaney-Bowers equation (Equation 1), g_{ave} = 3.68, 2*J* = -212 cm^{-1}.

$$\chi = \frac{\frac{2N\beta^2 g_{ave}^2 e^x}{kT} + \chi_{TIP}(1-e^x)}{(1+3e^x)} \text{ with } x = \frac{2J}{kT} \quad (1)$$

The curve was fitted by variating the 2*J* energy gap, which was then estimated to be -212 cm^{-1}. This was consistent with the triplet state being significantly populated at room temperature with k_BT = 203.7 cm^{-1} at 293.15 K. Considering that the χ_{TIP} and g_{ave} values were indicative of a high anisotropy, another model was developed by Lukens *et al.* to estimate the 2*J* energy gap for strongly coupled electrons.[69] To do so, they considered a two-state approximated wavefunction for the $Cp^*_2Yb(bipy)$ system: $\Psi = c_1|f^{13},bipy^{\bullet-}\rangle + c_2|f^{14},bipy^0\rangle$. By assuming that the Yb ion was purely trivalent f^{13}, c_1^2 was fixed to 1 and by injecting the g-tensor values of the similar $Cp^*_2Yb(bipy)^+$ cation in equation (2) (g_z = 7.05, g_y = 1.731 and g_x = 1.165),[68] 2*J* was then estimated to -202.6 cm^{-1}. Noteworthy, while the Bleaney-Bowers model usually tends to

overestimate the 2*J* value, the second one is likely to underestimate it. The fact that, in that case, both estimations were close to each other meant that the real electronic structure of **2** is close to the two-state approximated models used.

$$2\mathrm{J} = c_1^2 \frac{\mathrm{N}\beta^2}{6\chi_{\mathrm{TIP}}} \sum_{\mathrm{i=x,y,z}} \frac{\mathrm{g_J}(\mathrm{g_i} - \mathrm{g_{bipy^{\cdot -}}})^2}{\mathrm{g_i}(1 - \mathrm{g_J})}$$

$$\text{with } g_J = \frac{3}{2} + \frac{S(S+1) - L(L+1)}{2J(J+1)} \quad (2)$$

Because in the Pd case, the oxidative addition of MeI did not result in a change of ground state, the same result was expected with 3. However, the room temperature χT value of 2.67 cm^3 K mol^{-1} was indicative of a triplet state being populated, and upon temperature decrease, this value only went down to 1.31 cm^3 K mol^{-1} at 2 K due to the thermal depopulation of the crystal-field split states (Figure 6). The ground state of 3 was, therefore, a pure triplet (S = 1).

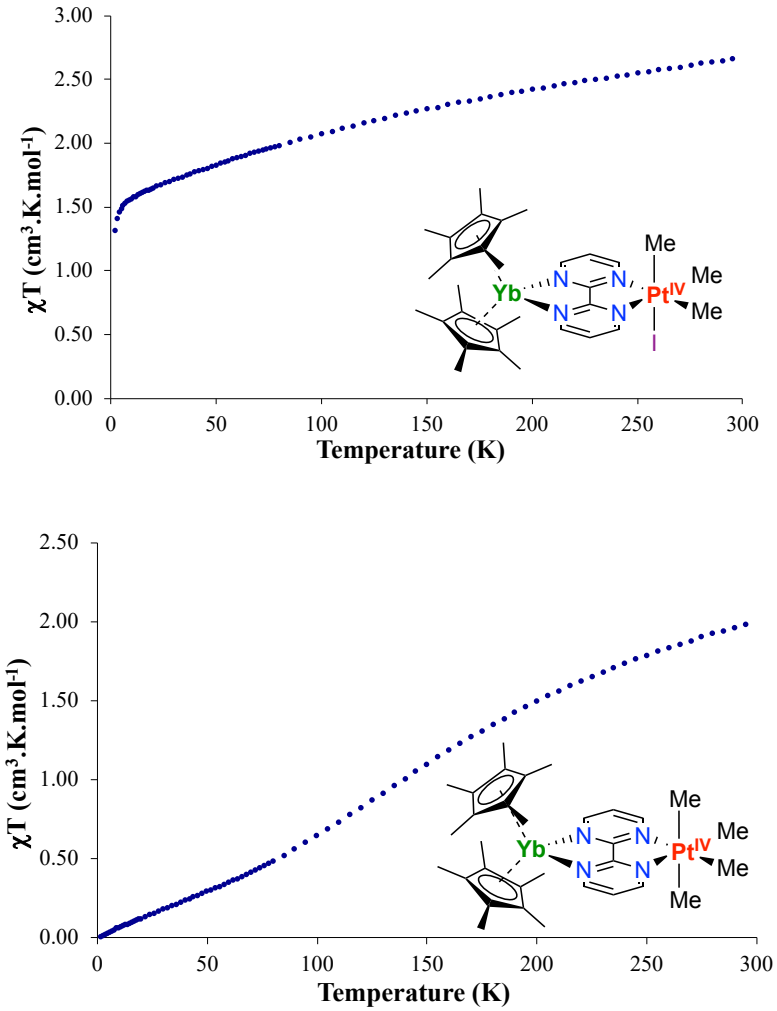

Figure 6. Solid-state temperature-dependent magnetic data of **3** (top) and **4** (bottom) recorded at 0.5 T: χT vs T plot.

Tuning the high-valent Pt coordinating environment

The electronic structure of **3** contrasts with that of the palladium analog, which was a singlet ground state.[36] To get more insights into this phenomenon, two other heterobimetallic Pt^{IV} species were targeted. First, thanks to the improved stability of **3** compared to its Pd analog, the substitution of the iodide in 3 by a fourth methyl ligand was investigated.[70,71] The thermal robustness of **3** allowed the addition of solid MeLi at room temperature to a solution of 3 in toluene. A slow color change of the solution from brown to dark red was observed, while an off-white solid appeared. After workup, XRD-suitable dark red prisms of $Cp^*_2Yb(bipym)PtMe_4$, **4**, were isolated in a 63 % yield (Figure 7). The overall metrics were slightly impacted by the substitution of the iodide for a methyl group. The C-C bond bridging the two pyrimidine rings was less than 0.01 Å longer in **4** than in **2** or **3** (1.41(1) Å versus 1.408(5) Å and 1.41(1) Å respectively). On the Yb side, the average Yb-Cp^*_{Ctr} distance of 2.29 Å was still in the trivalent range, and the most important changes were found on the Pt side. The Pt-N distance was 2.099(6) Å, which was significantly closer to the distance found in 2 (2.088(4) Å) than in 3 (2.15(1) Å). The average Pt-C distance was lengthened to 2.09(3) Å, which can be explained by the axial methyl groups being further (2.117(7) Å) than the equatorial ones (2.059(9) Å) (Table 1).

The ^{1}H NMR spectrum of **4** was acquired in thf-d_8 and presented the same typical paramagnetic behavior as 2 and 3. Only one Cp* peak was found at 6.03 ppm, which was indicative of a C_{2v} symmetry as expected with the substitution of the iodide by a methyl group. The bipym ligand peaks were found at 257.3, 3.40, and -164.9 ppm, while the methyl signals both integrating for 6 H were found at -2.71 ppm for the equatorial ones, *trans* to the bipym ligand and -15.01 ppm for the axial ones. This attribution was inherited from the respective axial and equatorial distribution of the peaks in **3** where the axial methyl group was found at -13.56 ppm while the equatorial ones were found at -0.43 ppm.

The solid-state magnetic measurements were conducted on **4**, and contrary to **3**, the χT versus T plot recorded at 0.5 T reaches a value close to 0 cm^3 K mol^{-1} at low temperature, meaning that 4 presented a singlet ground state (Figure 6). The value of χT at room temperature, 2.00 cm^3 K mol^{-1} indicated that a triplet state was populated but in a lesser proportion than what was observed in 2. To confirm this rapid observation, the 2*J* gap was estimated with the χ_{TIP} value being 0.00578 cm^3 mol^{-1}. This resulted in the modified Bleaney-Bowers model giving a value of -320 cm^{-1} with a g_{ave} fitted to 3.45, while the model from Lukens *et al.* resulted in a value of -252 cm^{-1}. Those values are somewhat different, which tended to indicate that our approximate model with only two states was not enough to fully describe the electronic structure of **4**. The possibility of multiple singlet states below the triplet state was already described.[27,28]

A third variant of high-valent Pt species with this heterobimetallic architecture was synthesized from MeOTf instead of MeI. The Pd^{IV} analog with the triflate anion could not be isolated. The structural characterization of the expected $Cp^*_2Yb(bipym)PtMe_3OTf$ complex, **5**, was achieved upon performing the oxidative addition in Et_2O. The product was found almost insoluble in this solvent, and a vapor diffusion of

MeOTf on a solution of 2 at -40 °C allowed the isolation of small yellow XRD-suitable needles that appeared within a few hours (Figure 7). The scaling up of the synthesis was achieved by the direct addition of MeOTf to a rapidly stirred Et_2O suspension of **2**. In C_6D6, the solubility of **5** is very low and features only one set of signals but with difficult attribution of the signals because of the low solubility. Thus, the ^1H NMR spectrum of **5** was performed in thf-d_8 (Figure S6). Several of the highly shifted bipym ligand resonances were split and were not integrating for the same values, indicating the presence of two structurally similar heterobimetallic species present in the solution.

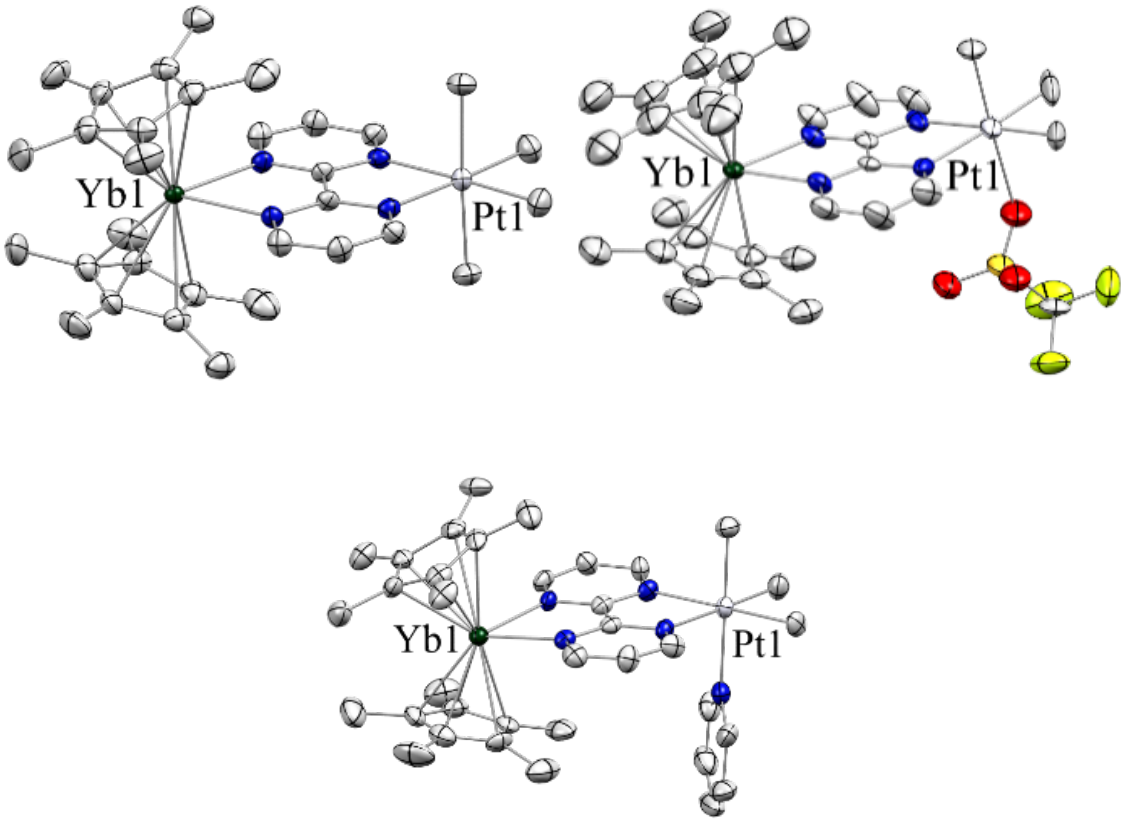

Figure 7. ORTEPs of complexes **4, 5**, and the **5^+(py)** cation with thermal ellipsoids at 50 % level. Carbon atoms are in grey, nitrogen atoms in blue, oxygen atoms in red, the sulfur atom in orange, fluorine atoms in yellow, the platinum atom in white, and the ytterbium atom in olive green. Hydrogen atoms have been removed for clarity.

Table 1. Main metric parameters in Å for the complexes **2-5** and **5⁺(py)OTf⁻**:

	2	**3**	**4**	**5**	**5⁺(py) OTf⁻**
C-C_{bipym}	1.408(5)	1.41(1)	1.41(1)	1.40(2)	1.41(1)
Pt-N_{bipym}	2.088(4)	2.15(1)	2.099(6)	2.150(9)	2.14(1)
Pt-C_{Me}	2.037(9)	2.06(4)	2.09(3)	2.03(3)	2.04(2)
Yb-Cp*$_{Ctr}$	2.31	2.36	2.29	2.29	2.30
Yb-N_{bipym}	2.361(3)	2.35(1)	2.363(6)	2.359(9)	2.35(3)

The overlapped Cp* signals were in agreement with the sum of two split Cp* signals as expected for C_s symmetry, while one other Cp* signal did not show any splitting. It is thus possible that the labile triflate anion can place itself in the equatorial position instead of the axial position in coordinating solvents, **5'**, modifying the symmetry of the complex. This ligand shuffle was observed with the oxidative addition at low temperatures of alkyl halides in strongly coordinating solvents such as acetone-d_6 or MeCN-d_3, but it was not reported with the oxidative addition of MeOTf in Et_2O on the 4,4'-^{t}Bu$_2$bipyPtMe$_2$ complex.[72] The other complex resulting from this ligand scrambling is also of C_s symmetry. However, the Cp* signal was not split, while the signals of the bipym ligand were. A reason why the splitting of the highly shifted bipym peaks of **5'** was not observed might result from them being overlapped.

The fact that both species were observable at the NMR time scale might mean that the dissociation of 5 in **5⁺(thf) OTf⁻** was the rate-limiting step of the isomerization equilibrium. While no crystal of the expected **5⁺(thf) OTf⁻** intermediate was isolated, when a stronger coordinating solvent, pyridine (py) was added to a toluene suspension of 5, the latter entirely displaced the triflate ligand. This led to the isolation of XRD suitable dark brown blocks of the [Cp*$_2$Yb(bipym)PdMe$_3$(py)]$^+$ OTf$^-$ compound, **5⁺(py) OTf⁻** (Figure 7).

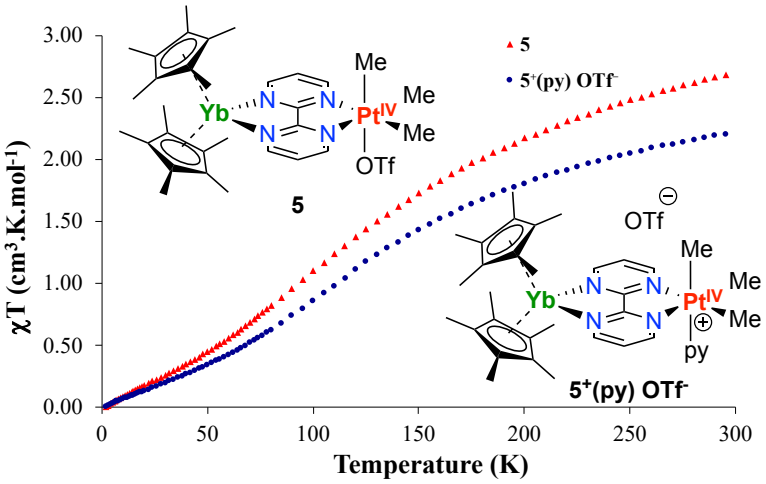

Figure 8. Solid-state temperature-dependent magnetic data of complexes **5** and **5$^+$(py) OTf$^-$** recorded at 0.5 T: χT vs T plot.

Both **5** and **5$^+$(py) OTf$^-$** were analyzed by SQUID magnetometry. Both χT versus T plot recorded at 0.5 T (Figure 8) revealed singlet ground states with rather similar room temperature χT values. For **5$^+$(py) OTf$^-$**, the χT value at room temperature was 2.22 cm^3 K mol^{-1}, meaning a 2J energy gap estimated to be between -237 cm^{-1} and -223 cm^{-1}, with the modified Bleaney-Bowers fit or the Lukens model.[69] For **5**, the room-temperature value was 2.71 cm^3 K mol^{-1}, a similar value to that of **3**, which featured a triplet ground state (2.68 cm^3 K mol^{-1}). The singlet-triplet energy gap was estimated, with the same methodology as before, to be between -238 cm^{-1} and -164 cm^{-1}. Thus, replacing the iodide anion with a triflate fragment led to a dramatic change to the ground state electronic structure. However, the lability of the triflate ion should increase the reactivity of the electrophilic Pt^{IV} center.

Reactivity studies.

In seminal studies, Puddephatt and coworkers showed that the light-induced reactivity of the (bipy)PtMe$_4$ complex resulted from the excitation of a Pt-C σ electron to the π* system of the bipy ligand.[70] As such, **4** was irradiated at 427 nm and monitored by ^{1}H NMR in C_6D_6. After two hours, the Cp* signal was split into two signals that were shifted from 5.84 ppm to 3.99 ppm and 3.14 ppm with close to 15 H integrations each. While this was indicative of the loss of the C_{2v} symmetry, the alkyl signals were also split into two sets and found at -3.00, and -4.72 ppm for the equatorial ones, and -14.39 and -16.19 ppm for the axial ones, all of them were integrated to 3 H. This meant that not only the equatorial symmetry plane found in 4 was broken, but also the axial one. Note that this transformation led to the only spectrum in which the $^2J(^{195}$Pt-CH) coupling constants were observed for such paramagnetic species and was typical of tetraalkyl platinum species, 74 Hz for the equatorial J(Pt-CH) and 43 Hz for the axial one.[73,74] In addition to these split

signals another set of 4 signals was growing at 57.81 ppm (1H), 39.49 ppm (1H), 28.29 (3H), 12.57 (1H). The fact that both Cp* signals and the four methyl signals were conserved also indicated that the transformation most likely occurred on the bipym ligand body. The formed species should, therefore, be a complex in which the bipym ligand would have been mono-functionalized by a methyl group $Cp^*_2Yb(Me\text{-}bipym)PtMe_4$, **4-hν** (Figure 9). Crystallization trials remained unsuccessful at different irradiation timing because it resulted in either recrystallization of starting complex 4 or isolation of polycrystalline samples that prevented any single crystal XRD analysis.

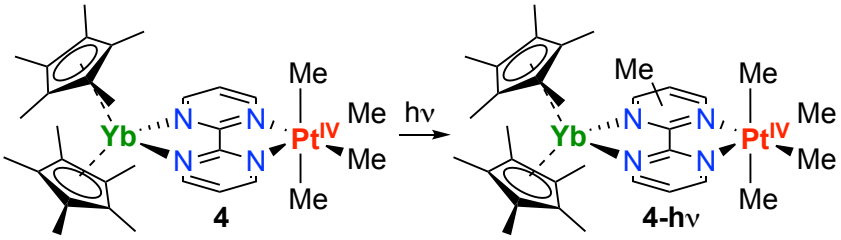

Figure 9. Proposed reactivity of **4** under irradiation.

In the case of **5**, several solvents, such as thf-d_8, C_6D_6, or tol-d_8, have been tested to monitor his stability over 18 hours at room temperature. At this time of the reaction, characteristic ^{1}H NMR signals of 4 slowly appeared upon the disappearance of **5**. This transformation was not quantitative and was attributed to a ligand exchange between two complexes **5** due to the lability of the triflate anion. Unfortunately, the other expected product from such transformation, a hypothetical $Cp^*_2Yb(bipym)PtMe_2(OTf)_2$ complex, was not observed nor isolated despite several crystallization attempts.

Similarly to Bercaw Labinger,[46] the abstraction of one methyl fragment was one obvious choice to increase the reactivity at the Pt^{II} center. Two strategies were pursued to obtain a hypothetical $[Cp^*_2Yb(bipym)PtMeL]^+$ cation, L being a neutral coordinating ligand: reaction with $B(C_6F_5)_3$ and with $[Ph_3C]^+[BPh_4]^-$.[75–78] Indeed, the typical addition of the Brookhart's acid used in seminal studies with platinum systems was incompatible with Cp^{*-} ligands. Both tests resulted in unexpected species, in which **2** was oxidized. On one hand, the reaction with $[Ph_3C]^+[BPh_4]^-$ led to a $\mathbf{2^+}$ $\mathbf{BPh_4^-}$ ionic pair, and the XRD analysis revealed a $C\text{-}C_{bipym}$ distance of 1.471(8) Å, indicating that the oxidation occurred on the bipym fragment. On the other hand, the reaction with $B(C_6F_5)_3$ assisted the Pt^{II} center in the activation of a thf-d_8 molecule - the solvent of the reaction, to form complex 6 (Figure 10)

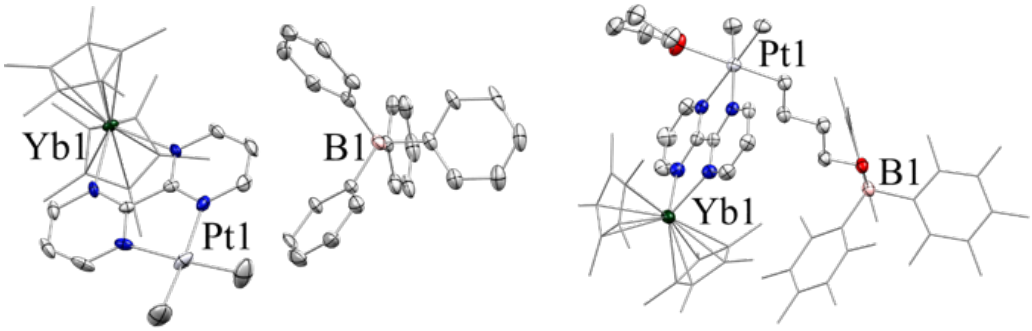

Figure 10. ORTEPs of the cation $\mathbf{2}^{+}$ and complex **6** with thermal ellipsoids at 50 % level. Carbon atoms are in grey, nitrogen atoms in blue, the platinum atom in white, and the ytterbium atom in olive green. Cp* and C_6F_5 ligands are represented in wireframe, while hydrogen atoms have been removed for clarity.

The formation of **6** may be understood as an FLP type of reactivity.[79,80] A comparative reaction with 1 and $B(C_6F_5)_3$ led to similar reactivity, although the transformation was slowed down. This was not surprising considering that the $Cp^*_2Yb(bipym)$ fragment enhanced the reaction rate by stabilizing the resulting Pt^{IV} center.[36] Such behavior with Pt^{II} was not reported. However, the FLP reactivity described herein remained of relative importance because similar reactions have already been reported with abundant metals.[81] The addition of the lanthanide fragment does not modify the fate of the reaction but only accelerates the rate. Trials in the absence of THF and in the presence of more valuable FLP-reactive substrates, such as H_2 or terminal alkynes,[82,83] should be pursued but are out of the scope of this article.

Conclusion

This article reports the synthesis of the $Cp^*_2Yb(bipym)PtMe_2$. Its oxidative reactivity was investigated, resulting in the isolation of a series of heterobimetallic complexes containing a high-valent Pt center. Among these species, one resulted from the activation of THF solvent by the FLP formed after the addition of $B(C_6F_5)_3$, an FLP reactivity that was not yet described with Pt^{II}. In previous works, the ground state of the heterobimetallic – and its reactivity were modified by the tuning of the bridging ligand between the lanthanide ion and the transition metal fragment. In this work, the ground state and the singlet-triplet energy gap are controlled by the Pt^{IV} coordination sphere. These findings open the way for state-selective reactivity with further ligand substitution, considering that small changes in the donating properties of such bidentate N-heteroaromatic ligands have already been shown to be crucial in platinum chemistry.

Experimental part

General considerations.

All reactions were performed using standard Schlenk-line techniques or a nitrogen-filled glovebox (MBraun). All glassware was dried at 140 °C for at least 12 h prior to use. Toluene, benzene, thf, tol-d_8, C_6D_6, thf-d_8 and pyridine were dried over sodium-benzophenone, degassed and transferred under reduced pressure in a cold flask. ^{1}H NMR spectra were recorded in 5 mm tubes adapted with a J. Young valve on Bruker Advance III at a Larmor frequency of 300 MHz. Chemical shifts are expressed relative to residual protio signal of the deuterated solvent in ppm.[84] Elemental analyses were obtained from Mikroanalytisches Labor Pascher (Remagen, Germany). Magnetic susceptibility measurements were made for all samples on a Quantum Design SQUID magnetometer (Cryogenic, London, UK). Diamagnetic corrections were made using Pascal's constants.[85] Temperature dependent magnetic measurements were obtained in sealed quartz tube on a Quantum Design SQUID under fixed DC fields between 0.1 and 2 T. "Curie tail" behavior at low temperature were corrected by considering the contribution of small Yb^{3+} impurities.[27,28] Infrared (IR) spectra were recorded at room temperature under argon on a Thermo Scientific Nicolet iS5 spectrometer equipped with the iD7 ATR – Diamond unit. UV-visible absorption spectra were recorded on a cary60 spectrometer in quartz cuvettes adapted with a J. Young valve. 2,2'-bipyrimidine was purchased from TCI and sublimed prior use. MeLi was purchased from Sigma Aldrich as a 1.6 M diethyl ether solution from which solid MeLi was obtained as a white powder after evaporation over several hours (10^{-3} mbar). $[Pt(SMe_2)Me_2]_2$, $(SMe_2)PtMeCl$ and Ph_3C^+ BPh_4^- were synthesized as described in the literature.[86,87] $B(C_6F_5)_3$ was purchased from Sigma Aldrich and used as received.

(bipym)PtMe$_2$ (**1**): Synthesis adapted from the literature.[56,57] To a colorless solution of 2,2'-bipyrimidine (250 mg, 1.58 mmol, 2 eq./Pt center) in CH_2Cl_2 (30 mL) a beige solution of $Pt_2(SMe_2)Me_4$ (230 mg, 0.4 mmol, 1 eq.) in CH_2Cl_2 (30 mL) was added dropwise under vigorous stirring. The solution slowly turns to deep red. After 2h of reaction, the dark red suspension is filtered through a frit to obtain a deep red solution and remove the black powder corresponding to the insoluble $[(bipym)Pt_2Me_4]$ dimer. The filtrate is then concentrated to a volume of 20 mL and covered with 70 mL of Et_2O and left to stand at – 20 °C. XRD suitable red needles are obtained overnight (190 mg, 0.50 mmol, 63%). A real care has to be taken to remove all remaining bipym ligand through this crystallization process since it will react with the lanthanide moiety in the further steps. **^{1}H NMR** (300 MHz, thf-d_8, 20 °C): δ (ppm)= 9.44 (m, 2H, bipym), 9.29 (m, 2H, bipym), 7.70 (t, 2H, bipym), 1.02 (s, 6H, Pt-CH_3, J_{Pt-H} = 87.5 Hz). **Anal. Calcd.** for $C_{10}H_{12}N_4Pt$: C, 31.33; H, 3.16; N, 14.62; found: C, 31.62; H, 3.27; N, 14.3.

Cp*$_2$Yb(bipym)PtMe$_2$(toluene) (**2**): To a red solution of $(bipym)PtMe_2$ (115 mg, 0.3 mmol, 1 eq.) in toluene (10 mL) a green solution of $Cp^*_2Yb(OEt_2)$ (158.3 mg, 0.3 mmol, 1 eq.) in toluene (10 mL) was added dropwise under vigorous stirring. After 5 min of reaction, the dark brownish-green solution was left at -40 °C overnight to yield dark crystals (217 mg, 0.26 mmol, 86%). **^{1}H NMR** (300 MHz, tol-d_8, 20 °C): δ (ppm) =

255.46 (s, 2H, bipym), 6.39 (s, 2H, bipym), -166.89 (s, 2H, bipym), 17.89 (s, 6H, Pt-CH_3), 5.88 (s, 30H, Cp*). **IR (ATR)**: ṽ = 2852, 2786, 1573, 1548, 1523, 1485, 1462, 1437, 1405, 1365, 1248, 1164, 1102, 1049, 1025, 987, 730, 680, 648 cm^{-1}. **Anal. Calcd.** for $C_{30}H_{42}N_4PtYb$ + C_7H_8: C, 48.36; H, 5.48; N, 6.10; found: C, 48.24; H, 5.52; N, 6.21.

Cp*$_2$Yb(bipym)PtMe$_3$I(toluene)$_{0.5}$ (**3**): To a dark green solution of Cp*$_2$Yb(bipym)PtMe$_2$ (166 mg, 0.18 mmol) in toluene (5 mL), two drops of MeI (excess) were added under vigorous stirring. The dark brownish-green solution turned instantly brown and was left stirring for 5min at room temperature before being left at -40 °C overnight to yield brown needles (167 mg, 0.16 mmol, 92%). **^{1}H NMR** (300 MHz, thf-d_8 ,20 °C): δ (ppm) = 266.18 (s, 2H, bipym), 13.25 (s, 2H, bipym), -187.50 (s, 2H, bipym), -0.24 (s, 6H, Pt-$(CH_3)_2$), -13.45 (s, 3H, Pt-CH_3), 6.47 (s, 15H, Cp*$_1$), 6.32 (s, 15H, Cp*$_2$). **IR (ATR)**: ṽ = 2893, 1558, 1473, 1405, 1372, 1300, 1243, 1225, 1204, 1170, 1015, 992, 750, 686, 634 cm^{-1}. **Anal. Calcd.** for $C_{31}H_{45}N_4IPtYb$ + $(C_7H_8)_{0.5}$: C, 40.83; H, 4.87; I, 12.51; N, 5.52; Pt, 19.22; Yb, 17.05; found: C, 40.61; H, 4.86; N, 5.32.

Cp*$_2$Yb(bipym)PtMe$_4$ (**4**): To a brown solution of Cp*$_2$Yb(bipym)PtMe$_3$I (56 mg, 55 µmol, 1eq.) in toluene (4 mL), solid MeLi (3.6 mg, 0.17 mmol, 3 eq.) was added at room temperature under vigorous stirring. The resulting suspension slowly turned dark red over several hours and was filtered after 24 h of stirring. The resulting solution was concentrated under vacuum and left overnight at -40 °C to yield XRD suitable dark red prisms (33 mg, 35 µmol, 63%). **^{1}H NMR** (300 MHz, thf-d_8 ,20 °C): δ (ppm) = 257.28 (s, 2H, bipym), 3.40 (s, 2H, bipym), -164.91 (s, 2H, bipym), -2.71 (s, 6H, Pt-$(CH_3)_2$), -15.01 (s, 6H, Pt-$(CH_3)_2$), 6.03 (s, 30H, Cp*). **IR (ATR)**: ṽ = 2903, 2851, 1557, 1521, 1486, 1461, 1438, 1406, 1368, 1267, 1245, 1162, 1099, 1046, 1022, 982, 965, 814, 737, 681 cm^{-1}. No satisfactory EA was obtained.

Cp*$_2$Yb(bipym)PtMe$_3$OTf (**5**): To a dark green suspension of Cp*$_2$Yb(bipym)PtMe$_2$ (240 mg, 0.26 mmol) in Et_2O (8 mL), four drops of MeOTf (excess) were added under vigorous stirring. The dark brownish-green solution rapidly turned to a yellow-brown suspension and was left stirring for 15 min at room temperature before being left at -40 °C overnight to yield a brown microcrystalline powder (251 mg, 0.25 mmol, 96%). XRD suitable crystals were grown by gas phase slow diffusion of MeOTf over a solution of Cp*$_2$Yb(bipym)PtMe$_2$ in Et_2O. **^{1}H NMR** was recorded in thf-d_8 at 20 °C and showed the presence of two isomers (Figure S6). **IR (ATR)**: ṽ = 2894, 1563, 1476, 1417, 1374, 1300, 1226, 1206, 1169, 1016, 994, 772, 685, 635 cm^{-1}. **Anal. Calcd.** for $C_{32}H_{45}F_3N_4O_3PtSYb$: C, 38.79; H, 4.58; N, 5.65; found: C, 39.15; H, 4.71; N, 5.54.

[Cp*$_2$Yb(bipym)Pt(py)Me$_3$]$^+$OTf$^-$(toluene) (**5$^+$(py) OTf$^-$**): To a yellow-brown suspension of Cp*$_2$Yb(bipym)PtMe$_3$OTf (58 mg, 59 µmol) in toluene (5 mL), four drops of pyridine (excess) were added at -40 °C and left to diffuse slowly at room temperature. The solution slowly turned deep red and dark XRD suitable crystals started to appear. The product was isolated after concentration of the solution to ~ 1 mL (53 mg, 0.046 mmol, 78%). **^{1}H NMR** (300 MHz, pyridine-d_5 ,20 °C): δ (ppm) = 269.09 (s, 2H, bipym), 26.41 (s, 2H, bipym), -213.91 (s, 2H, bipym), 2.50 (s, 6H, Pt-$(CH_3)_2$), -14.05 (s, 3H, Pt-CH_3), 6.85 (s, 15H, Cp*$_1$), 6.55

(s, 15H, Cp^*_2). **IR (ATR)**: ṽ = 2961, 2898, 2862, 2604, 1564, 1489, 1474, 1447, 1437, 1407, 1374, 1264, 1222, 1173, 1152, 1066, 1031, 760, 703, 637 cm^{-1}. **Anal. Calcd.** for $C_{39.1}H_{52.4}F_3N_5O_3PtSYb+ (C_7H_8)_{0.5}$: C, 42.78; H, 4.81; N, 6.38 found: C, 42.65; H, 4.78; N, 6.38. Approximately 0.7 molecules of toluene removed upon drying.

Reactivity of complex 2 with Ph_3C^+ BPh_4^-: To a dark green solution of $Cp^*_2Yb(bipym)PtMe_2$ (5 mg, 5 µmol) in thf-d_8 (0.4 mL), solid Ph_3C^+ BPh_4^- (excess) was added. The solution immediately turned dark brown and XRD suitable needles of the same color appeared in few minutes at room temperature. **^{1}H NMR** (300 MHz, thf-d_8 ,20 °C): δ (ppm) = 249.47 (s, 2H, bipym), 10.06 (s, 2H, bipym), -124.35 (s, 2H, bipym), 13.75 (s, 6H, Pt-$(CH_3)_2$), 5.47 (s, 30H, Cp*), 14.69 (s, 8H, BPh_4), 12.36 (s, 8H, BPh_4), 11.20 (s, 4H, BPh_4).

Reactivity of complex 2 with $B(C_6F_5)_3$: To a dark green solution of $Cp^*_2Yb(bipym)PtMe_2$ (8 mg, 0.009 mmol, 1 eq.) in thf-d_8 (0.4 mL), solid $B(C_6F_5)_3$ (4.2 mg, 0.009 mmol, 1 eq.) was added. The solution immediately turned dark brown and XRD suitable plates of the same color appeared in few minutes at room temperature. **^{1}H NMR** (300 MHz, thf-d_8 ,20 °C): δ (ppm) = 273.95 (s, 2H, bipym), 27.93 (s, 2H, bipym), -216.59 (s, 2H, bipym), 5.94 (s, 6H, Pt-$(CH_3)_2$), 6.66 (s, 15H, Cp^*_1), 6.28 (s, 15H, Cp^*_2).

Associated Content

Supporting Information. Details on the solution NMR and X-ray crystallography (PDF). This material is available free of charge via the Internet at http://pubs.acs.org. The crystal structures of **2** to **6, 5^+(py) OTf^-** and **2^+ BPh_4^-** have been deposited in the CCDC with #2369155-2369161

Authors information

Corresponding Author

* gregory.danoun@polytechnique.edu

* gregory.nocton@polytechnique.edu

Acknowledgment

This project has received funding from the European Research Council (ERC) under the European Union's Horizon (H2020) research program (grant agreement number 716314). CNRS and Ecole polytechnique are thanked for funding.

References

(1) Benelli, C.; Gatteschi, D. Introduction to Molecular Magnetism: From Transition Metals to Lanthanides; 2015; p 71.

(2) Wang, L.; Zhao, Z.; Wei, C.; Wei, H.; Liu, Z.; Bian, Z.; Huang, C. Review on the Electroluminescence Study of Lanthanide Complexes. *Adv Opt Mater* **2019**, *7* (11), 1801256. https://doi.org/https://doi.org/10.1002/adom.201801256.

(3) Straub, B. F. Organotransition Metal Chemistry. From Bonding to Catalysis. Edited by John F. Hartwig.; 2010; Vol. 49. https://doi.org/10.1002/anie.201004890.

(4) Teegardin, K.; Day, J. I.; Chan, J.; Weaver, J. Advances in Photocatalysis: A Microreview of Visible Light Mediated Ruthenium and Iridium Catalyzed Organic Transformations. *Org Process Res Dev* **2016**, *20* (7), 1156–1163. https://doi.org/10.1021/acs.oprd.6b00101.

(5) Sarkar, S.; Cheung, K. P. S.; Gevorgyan, V. Recent Advances in Visible Light Induced Palladium Catalysis. *Angewandte Chemie International Edition* **2024**, *63* (9), e202311972. https://doi.org/https://doi.org/10.1002/anie.202311972.

(6) Kahn, O. Spin-Crossover Molecular Materials. *Curr Opin Solid State Mater Sci* **1996**, *1* (4), 547–554. https://doi.org/https://doi.org/10.1016/S1359-0286(96)80070-2.

(7) Gütlich, P. Spin Crossover – Quo Vadis? *Eur J Inorg Chem* **2013**, *2013* (5–6), 581–591. https://doi.org/https://doi.org/10.1002/ejic.201300092.

(8) Schröder, D.; Shaik, S.; Schwarz, H. Two-State Reactivity as a New Concept in Organometallic Chemistry. *Acc Chem Res* **2000**, *33* (3), 139–145. https://doi.org/10.1021/ar990028j.

(9) Dhuri, S. N.; Seo, M. S.; Lee, Y.-M.; Hirao, H.; Wang, Y.; Nam, W.; Shaik, S. Experiment and Theory Reveal the Fundamental Difference between Two-State and Single-State Reactivity Patterns in Nonheme FeIV□O versus RuIV□O Oxidants. *Angewandte Chemie International Edition* **2008**, *47* (18), 3356–3359. https://doi.org/https://doi.org/10.1002/anie.200705880.

(10) Klinker, E. J.; Shaik, S.; Hirao, H.; Que Jr., L. A Two-State Reactivity Model Explains Unusual Kinetic Isotope Effect Patterns in C□H Bond Cleavage by Nonheme Oxoiron(IV) Complexes. *Angewandte Chemie International Edition* **2009**, *48* (7), 1291–1295. https://doi.org/https://doi.org/10.1002/anie.200804029.

(11) Cooper, B. G.; Napoline, J. W.; Thomas, C. M. Catalytic Applications of Early/Late Heterobimetallic Complexes. *Catalysis Reviews* **2012**, *54* (1), 1–40. https://doi.org/10.1080/01614940.2012.619931.

(12) Buchwalter, P.; Rosé, J.; Braunstein, P. Multimetallic Catalysis Based on Heterometallic Complexes and Clusters. *Chem Rev* **2015**, *115* (1), 28–126. https://doi.org/10.1021/cr500208k.

(13) Lassalle, S.; Jabbour, R.; Schiltz, P.; Berruyer, P.; Todorova, T. K.; Veyre, L.; Gajan, D.; Lesage, A.; Thieuleux, C.; Camp, C. Metal–Metal Synergy in Well-Defined Surface Tantalum–Iridium Heterobimetallic Catalysts for H/D Exchange Reactions. *J Am Chem Soc* **2019**, *141* (49), 19321–19335. https://doi.org/10.1021/jacs.9b08311.

(14) Affronte, M.; Carretta, S.; Timco, G. A.; Winpenny, R. E. P. A Ring Cycle: Studies of Heterometallic Wheels. *Chemical Communications* **2007**, No. 18, 1789–1797. https://doi.org/10.1039/B615543J.

(15) Feltham, H. L. C.; Brooker, S. Review of Purely 4f and Mixed-Metal Nd-4f Single-Molecule Magnets Containing Only One Lanthanide Ion. *Coord Chem Rev* **2014**, *276*, 1–33. https://doi.org/https://doi.org/10.1016/j.ccr.2014.05.011.

(16) Tan, X.; Ji, X.; Zheng, J.-M. Heterometallic Tetranuclear 3d–4f Complexes: Syntheses, Structures and Magnetic Properties. *Inorg Chem Commun* **2015**, *60*, 27–32. https://doi.org/https://doi.org/10.1016/j.inoche.2015.07.027.

(17) Liu, K.; Shi, W.; Cheng, P. Toward Heterometallic Single-Molecule Magnets: Synthetic Strategy, Structures and Properties of 3d–4f Discrete Complexes. *Coord Chem Rev* **2015**, *289–290*, 74–122. https://doi.org/https://doi.org/10.1016/j.ccr.2014.10.004.

(18) Alsowayigh, M. M.; Timco, G. A.; Borilovic, I.; Alanazi, A.; Vitorica-yrezabal, I. J.; Whitehead, G. F. S.; McNaughter, P. D.; Tuna, F.; O'Brien, P.; Winpenny, R. E. P.; Lewis, D. J.; Collison, D. Heterometallic 3d–4f Complexes as Air-Stable Molecular Precursors in Low Temperature Syntheses of Stoichiometric Rare-Earth Orthoferrite Powders. *Inorg Chem* **2020**, *59* (21), 15796–15806. https://doi.org/10.1021/acs.inorgchem.0c02249.

(19) Cotton, S. A. *Lanthanide and Actinide Chemistry*; Wiley: Chichester, England; Hoboken, NJ, 2006.

(20) Birmingham, J. M.; Wilkinson, G. The Cyclopentadienides of Scandium, Yttrium and Some Rare Earth Elements. *J Am Chem Soc* **1956**, *78* (1), 42–44. https://doi.org/10.1021/ja01582a009.

(21) Fischer, E. O.; Fischer, H. Uber Dicyclopentadienyleuropium Und Dicyclopentadienylytterbium Und Tricyclopentadienyle Des Terbiums, Holmiums, Thuliums Und Lutetiums. *J Organomet Chem* **1965**, *3* (3), 181–187. https://doi.org/https://doi.org/10.1016/S0022-328X(00)87500-2.

(22) Apostolidis, C.; Deacon, G. B.; Dornberger, E.; Edelmann, F. T.; Kanellakopulos, B.; MacKinnon, P.; Stalke, D. Crystallization and X-Ray Structures of [NaYb(C5H5)3] and Yb(C5H5)2. *Chemical Communications* **1997**, No. 11, 1047–1048. https://doi.org/10.1039/A700531H.

(23) Eggers, S. H.; Kopf, J.; Fischer, R. D. Structure of Tris(H5-Cyclopentadienyl)Ytterbium(III). *Acta Crystallographica Section C* **1987**, *43* (12), 2288–2290. https://doi.org/10.1107/S0108270187088036.

(24) Denning, R. G.; Harmer, J.; Green, J. C.; Irwin, M. Covalency in the 4f Shell of Tris-Cyclopentadienyl Ytterbium (YbCp3)—A Spectroscopic Evaluation. *J Am Chem Soc* **2011**, *133* (50), 20644–20660. https://doi.org/10.1021/ja209311g.

(25) Greco, A.; Cesca, S.; Bertolini, W. New π-Cyclooctatetraenyl and π-Cyclopentadienyl Complexes of Cerium. *J Organomet Chem* **1976**, *113* (4), 321–330. https://doi.org/https://doi.org/10.1016/S0022-328X(00)96143-6.

(26) Walter, M. D.; Booth, C. H.; Lukens, W. W.; Andersen, R. A. Cerocene Revisited: The Electronic Structure of and Interconversion Between Ce2(C8H8)3 and Ce(C8H8)2. *Organometallics* **2009**, *28* (3), 698–707. https://doi.org/10.1021/om7012327.

(27) Booth, C. H.; Walter, M. D.; Kazhdan, D.; Hu, Y.-J.; Lukens, W. W.; Bauer, E. D.; Maron, L.; Eisenstein, O.; Andersen, R. A. Decamethylytterbocene Complexes of Bipyridines and Diazabutadienes: Multiconfigurational Ground States and Open-Shell Singlet Formation. *J Am Chem Soc* **2009**, *131* (18), 6480–6491. https://doi.org/10.1021/ja809624w.

(28) Booth, C. H.; Kazhdan, D.; Werkema, E. L.; Walter, M. D.; Lukens, W. W.; Bauer, E. D.; Hu, Y.-J.; Maron, L.; Eisenstein, O.; Head-Gordon, M.; Andersen, R. A. Intermediate-Valence Tautomerism in Decamethylytterbocene Complexes of Methyl-Substituted Bipyridines. *J Am Chem Soc* **2010**, *132* (49), 17537–17549. https://doi.org/10.1021/ja106902s.

(29) Kerridge, A. Oxidation State and Covalency in F-Element Metallocenes (M = Ce, Th, Pu): A Combined CASSCF and Topological Study. *Dalton Transactions* **2013**, *42* (46), 16428–16436. https://doi.org/10.1039/C3DT52279B.

(30) Mooßen, O.; Dolg, M. Two Interpretations of the Cerocene Electronic Ground State. **2014**. https://doi.org/10.1016/j.cplett.2014.01.022.

(31) Tricoire, M.; Mahieu, N.; Simler, T.; Nocton, G. Intermediate Valence States in Lanthanide Compounds. *Chemistry – A European Journal* **2021**, *27* (23), 6860–6879. https://doi.org/https://doi.org/10.1002/chem.202004735.

(32) Nocton, G.; Booth, C. H.; Maron, L.; Andersen, R. A. Influence of the Torsion Angle in 3,3′-Dimethyl-2,2′-Bipyridine on the Intermediate Valence of Yb in (C5Me5)2Yb(3,3′-Me2-Bipy). *Organometallics* **2013**, *32* (19), 5305–5312. https://doi.org/10.1021/om400528d.

(33) Nocton, G.; Booth, C. H.; Maron, L.; Andersen, R. A. Thermal Dihydrogen Elimination from Cp*2Yb(4,5-Diazafluorene). *Organometallics* **2013**, *32* (5), 1150–1158. https://doi.org/10.1021/om300876b.

(34) Nocton, G.; Booth, C. H.; Maron, L.; Ricard, L.; Andersen, R. A. Carbon–Hydrogen Bond Breaking and Making in the Open-Shell Singlet Molecule Cp*2Yb(4,7-Me2phen). *Organometallics* **2014**, *33* (23), 6819–6829. https://doi.org/10.1021/om500843z.

(35) Nocton, G.; Lukens, W. W.; Booth, C. H.; Rozenel, S. S.; Medling, S. A.; Maron, L.; Andersen, R. A. Reversible Sigma C-C Bond Formation between Phenanthroline Ligands Activated by (C5Me5)2Yb. *J Am Chem Soc* **2014**, *136* (24), 8626–8641. https://doi.org/10.1021/ja502271q.

(36) Goudy, V.; Jaoul, A.; Cordier, M.; Clavaguéra, C.; Nocton, G. Tuning the Stability of Pd(IV) Intermediates Using a Redox Non-Innocent Ligand Combined with an Organolanthanide Fragment. *J Am Chem Soc* **2017**, *139* (31), 10633–10636. https://doi.org/10.1021/jacs.7b05634.

(37) Wang, D.; Moutet, J.; Tricoire, M.; Cordier, M.; Nocton, G. Reactive Heterobimetallic Complex Combining Divalent Ytterbium and Dimethyl Nickel Fragments. *Inorganics (Basel)* **2019**, *7* (5), 58. https://doi.org/10.3390/inorganics7050058.

(38) Jaoul, A.; Tricoire, M.; Moutet, J.; Cordier, M.; Clavaguéra, C.; Nocton, G. Reversible Electron Transfer in Organolanthanide Chemistry. *Chem Sq* **2019**, *3*, 1. https://doi.org/10.28954/2019.csq.06.001.

(39) Wang, D.; Tricoire, M.; Cemortan, V.; Moutet, J.; Nocton, G. Redox Activity of a Dissymmetric Ligand Bridging Divalent Ytter-Bium and Reactive Nickel Fragments. *Inorg Chem Front* **2021**, *8* (3), 647–657. https://doi.org/10.1039/D0QI00952K.

(40) Cemortan, V.; Simler, T.; Moutet, J.; Jaoul, A.; Clavaguéra, C.; Nocton, G. Structure and Bonding Patterns in Heterometallic Organometallics with Linear Ln–Pd–Ln Motifs. *Chem. Sci.* **2023**, *14* (10), 2676–2685. https://doi.org/10.1039/D2SC06933D.

(41) Tricoire, M.; Wang, D.; Rajeshkumar, T.; Maron, L.; Danoun, G.; Nocton, G. Electron Shuttle in N-Heteroaromatic Ni Catalysts for Alkene Isomerization. *JACS Au* **2022**, *2* (8), 1881–1888. https://doi.org/10.1021/jacsau.2c00251.

(42) Shilov, A. E.; Shul'pin, G. B. Activation of C−H Bonds by Metal Complexes. *Chem Rev* **1997**, *97* (8), 2879–2932. https://doi.org/10.1021/cr9411886.

(43) Shilov, A. E.; Shteinman, A. A. Activation of Saturated Hydrocarbons by Metal Complexes in Solution. *Coord Chem Rev* **1977**, *24* (2–3), 97–143. https://doi.org/10.1016/S0010-8545(00)80336-7.

(44) Labinger, J. A.; Bercaw, J. E. Mechanistic Studies on the Shilov System: A Retrospective. *J Organomet Chem* **2015**, *793*, 47–53. https://doi.org/https://doi.org/10.1016/j.jorganchem.2015.01.027.

(45) Stahl, S. S.; Labinger, J. A.; Bercaw, J. E. Exploring the Mechanism of Aqueous C−H Activation by Pt(II) through Model Chemistry: Evidence for the Intermediacy of Alkylhydridoplatinum(IV) and Alkane σ-Adducts. *J Am Chem Soc* **1996**, *118* (25), 5961–5976. https://doi.org/10.1021/ja960110z.

(46) Holtcamp, M. W.; Labinger, J. A.; Bercaw, J. E. C−H Activation at Cationic Platinum(II) Centers. *J Am Chem Soc* **1997**, *119* (4), 848–849. https://doi.org/10.1021/ja9620595.

(47) Periana, R. A.; Taube, D. J.; Gamble, S.; Taube, H.; Satoh, T.; Fujii, H. Platinum Catalysts for the High-Yield Oxidation of Methane to a Methanol Derivative. *Science (1979)* **1998**, *280* (5363), 560–564. https://doi.org/10.1126/science.280.5363.560.

(48) Kua, J.; Xu, X.; Periana, R. A.; Goddard, W. A. Stability and Thermodynamics of the PtCl2 Type Catalyst for Activating Methane to Methanol: A Computational Study. *Organometallics* **2002**, *21* (3), 511–525. https://doi.org/10.1021/om0101691.

(49) Xu, X.; Kua, J.; Periana, R. A.; Goddard, W. A. Structure, Bonding, and Stability of a Catalytica Platinum(II) Catalyst: A Computational Study. *Organometallics* **2003**, *22* (10), 2057–2068. https://doi.org/10.1021/om0202165.

(50) Villalobos, J. M.; Hickman, A. J.; Sanford, M. S. Platinum(II) Complexes Containing Quaternized Nitrogen Ligands: Synthesis, Stability, and Evaluation as Catalysts for Methane and Benzene H/D Exchange. *Organometallics* **2010**, *29* (1), 257–262. https://doi.org/10.1021/om900889k.

(51) Rendina, L. M.; Puddephatt, R. J. Oxidative Addition Reactions of Organoplatinum(II) Complexes with Nitrogen-Donor Ligands. *Chem Rev* **1997**, *97* (6), 1735–1754. https://doi.org/10.1021/cr9704671.

(52) Byers, P. K.; Canty, A. J.; Skelton, B. W.; White, A. H.; Whitelb, A. H. Synthesis, Reactivity, and Structural Studies in Trimethylpalladium(IV) Chemistry, Including PdIMe3(Bpy) and [MMe3((Pz)3CH)]+ (M = Palladium, Platinum). *Organometallics* **1990**, *9* (3), 826–832. https://doi.org/10.1021/om00117a044.

(53) Canty, A. J.; Gardiner, M. G.; Jones, R. C.; Rodemann, T.; Sharma, M. Binuclear Intermediates in Oxidation Reactions: [(Me3SiC≡ C)Me2(Bipy)Pt-PtMe2(Bipy)]+ in the Oxidation of PtIIMe2(Bipy) (Bipy = 2,2′-Bipyridine) by IPh(C≡CSiMe3)(OTf) (OTf = Triflate). *J Am Chem Soc* **2009**, *131* (21), 7236–7237. https://doi.org/10.1021/ja902799u.

(54) Scott, J. D.; Puddephatt, R. J. Ligand Dissociation as a Preliminary Step in Methyl-for-Halogen Exchange Reactions of Platinum(II) Complexes. *Organometallics* **1983**, *2* (11), 1643–1648. https://doi.org/10.1021/om50005a028.

(55) Sutcliffe, V. F.; Young, G. B. Organometallic and Organobimetallic Complexes of Platinum(II) Containing 2,2′-Bipyrimidyl: Syntheses and Spectroscopic Characteristics. *Polyhedron* **1984**, *3* (1), 87–94. https://doi.org/10.1016/S0277-5387(00)84718-X.

(56) Scott, J. D.; Puddephatt, R. J. Binuclear and Tetranuclear Mixed Oxidation State Platinum Complexes Containing Both μ-2,2′-Bipyrimidine and μ-Hydrocarbyl Ligands. *Organometallics* **1986**, *5* (8), 1538–1544. https://doi.org/10.1021/om00139a005.

(57) Mironov, O. A.; Bischof, S. M.; Konnick, M. M.; Hashiguchi, B. G.; Ziatdinov, V. R.; Goddard, W. A.; Ahlquist, M. M.; Periana, R. A. Using Reduced Catalysts for Oxidation Reactions: Mechanistic Studies of the "Periana-Catalytica" System for CH4 Oxidation. *J Am Chem Soc* **2013**, *135* (39), 14644–14658. https://doi.org/10.1021/ja404895z.

(58) Berg, D. J.; Boncella, J. M.; Andersen, R. A. Preparation of Coordination Compounds of Cp*2Yb with Heterocyclic Nitrogen Bases: Examples of Antiferromagnetic Exchange Coupling across Bridging Ligands. *Organometallics* **2002**, *21* (22), 4622–4631. https://doi.org/10.1021/om020477e.

(59) Gould, C. A.; Mu, E.; Vieru, V.; Darago, L. E.; Chakarawet, K.; Gonzalez, M. I.; Demir, S.; Long, J. R. Substituent Effects on Exchange Coupling and Magnetic Relaxation in 2,2′-Bipyrimidine Radical-Bridged Dilanthanide Complexes. *J Am Chem Soc* **2020**, *142* (50), 21197–21209. https://doi.org/10.1021/jacs.0c10612.

(60) Modder, D. K.; Batov, M. S.; Rajeshkumar, T.; Sienkiewicz, A.; Zivkovic, I.; Scopelliti, R.; Maron, L.; Mazzanti, M. Assembling Diuranium Complexes in Different States of Charge with a Bridging Redox-Active Ligand. *Chem. Sci.* **2022**, *13* (38), 11294–11303. https://doi.org/10.1039/D2SC03592H.

(61) Schultz, M.; Boncella, J. M.; Berg, D. J.; Tilley, T. D.; Andersen, R. A. Coordination of 2,2‘-Bipyridyl and 1,10-Phenanthroline to Substituted Ytterbocenes: An Experimental Investigation of Spin Coupling in Lanthanide Complexes. *Organometallics* **2002**, *21* (3), 460–472. https://doi.org/10.1021/om010661k.

(62) Nabavizadeh, S. M.; Habibzadeh, S.; Rashidi, M.; Puddephatt, R. J. Oxidative Addition of Ethyl Iodide to a Dimethylplatinum(II) Complex: Unusually Large Kinetic Isotope Effects and Their Transition-State Implications. *Organometallics* **2010**, *29* (23), 6359–6368. https://doi.org/10.1021/om100810t.

(63) Nasser, N.; Fard, M. A.; Boyle, P. D.; Puddephatt, R. J. Oxygen Atom Transfer to Platinum(II): A 2-Pyridyloxaziridine and a 2-Pyridylnitrone as Potential Oxygen Atom Donors. *J Organomet Chem* **2018**, *858*, 67–77. https://doi.org/https://doi.org/10.1016/j.jorganchem.2017.12.043.

(64) Mala, B.; Murtagh, L. E.; Farrow, C. M. A.; Akien, G. R.; Halcovich, N. R.; Allinson, S. L.; Platts, J. A.; Coogan, M. P. Photochemical Oxidation of Pt(IV)Me3(1,2-Diimine) Thiolates to Luminescent Pt(IV) Sulfinates. *Inorg Chem* **2021**, *60* (10), 7031–7043. https://doi.org/10.1021/acs.inorgchem.0c03553.

(65) Walter, M. D.; Berg, D. J.; Andersen, R. A. Coordination Complexes of Decamethylytterbocene with 4,4'-Disubstituted Bipyridines: An Experimental Study of Spin Coupling in Lanthanide Complexes. *Organometallics* **2006**, *25* (13), 3228–3237. https://doi.org/10.1021/om051051d.

(66) Van Vleck, J. H. *The Theory of Electric and Magnetic Susceptibilities*; International series of monographs on physics; Oxford University Press, 1965.

(67) O'Connor, C. J. Magnetochemistry—Advances in Theory and Experimentation. *Progress in Inorganic Chemistry*. January 1, 1982, pp 203–283. https://doi.org/https://doi.org/10.1002/9780470166307.ch4.

(68) Lukens, W. W.; Walter, M. D. Quantifying Exchange Coupling in F-Ion Pairs Using the Diamagnetic Substitution Method. *Inorg Chem* **2010**, *49* (10), 4458–4465. https://doi.org/10.1021/ic100120d.

(69) Lukens, W. W.; Magnani, N.; Booth, C. H. Application of the Hubbard Model to Cp*2Yb(Bipy), a Model System for Strong Exchange Coupling in Lanthanide Systems. *Inorg Chem* **2012**, *51* (19), 10105–10110. https://doi.org/10.1021/ic300037q.

(70) Hux, J. E.; Puddephatt, R. J. Photochemistry of Tetramethyl(2,2'-Bipyridine)Platinum(IV). *J Organomet Chem* **1988**, *346* (1), C31–C34. https://doi.org/10.1016/0022-328X(88)87020-7.

(71) Hux, J. E.; Puddephatt, R. J. Photochemistry of Mononuclear and Binuclear Tetramethylplatinum(IV) Complexes: Reactivity of an Organometallic Free Radical. *J Organomet Chem* **1992**, *437* (1), 251–263. https://doi.org/https://doi.org/10.1016/0022-328X(92)83448-Q.

(72) Hill, G. S.; Puddephatt, R. J. Methyl(Hydrido)Platinum(IV) Complexes That Are Resistant to Reductive Elimination, Including the First (μ-Hydrido)Diplatinum(IV) Complex. *J Am Chem Soc* **1996**, *118* (36), 8745–8746. https://doi.org/10.1021/ja961404n.

(73) Clegg, D. E.; Hall, J. R.; Swile, G. A. 1H NMR Spectra and Characterization of Some Trimethylplatinum(IV) Compounds: Evidence for Cis and Trans Influences. *J Organomet Chem* **1972**, *38* (2), 403–420. https://doi.org/https://doi.org/10.1016/S0022-328X(00)83343-4.

(74) Hux, J. E.; Puddephatt, R. J. Reactivity of Tetramethylplatinum(IV) Complexes: Thermal Reactions with Electrophiles and Unsaturated Reagents. *Inorganica Chim Acta* **1985**, *100* (1), 1–5. https://doi.org/https://doi.org/10.1016/S0020-1693(00)88287-0.

(75) Bochmann, M.; Lancaster, S. J. Base-Free Cationic 14-Electron Alkyls of Ti, Zr and Hf as Polymerisation Catalysts: A Comparison. *J Organomet Chem* **1992**, *434* (1), C1–C5. https://doi.org/https://doi.org/10.1016/0022-328X(92)83360-T.

(76) Hill, G. S.; Rendina, L. M.; Puddephatt, R. J. Cationic Platinum(II) Complexes: Platinum–Alkyl Bond Cleavage by a Powerful Lewis Acid. *Journal of the Chemical Society, Dalton Transactions* **1996**, No. 9, 1809–1813. https://doi.org/10.1039/DT9960001809.

(77) Piers, W. E.; Chivers, T. Pentafluorophenylboranes: From Obscurity to Applications. *Chem Soc Rev* **1997**, *26* (5), 345–354. https://doi.org/10.1039/CS9972600345.

(78) Campos, J.; López-Serrano, J.; Peloso, R.; Carmona, E. Methyl Complexes of the Transition Metals. *Chemistry – A European Journal* **2016**, *22* (19), 6432–6457. https://doi.org/https://doi.org/10.1002/chem.201504483.

(79) Chapman, A. M.; Haddow, M. F.; Wass, D. F. Frustrated Lewis Pairs beyond the Main Group: Synthesis, Reactivity, and Small Molecule Activation with Cationic Zirconocene–Phosphinoaryloxide Complexes. *J Am Chem Soc* **2011**, *133* (45), 18463–18478. https://doi.org/10.1021/ja207936p.

(80) Zhao, X.; Lough, A. J.; Stephan, D. W. Synthesis and Reactivity of Alkynyl-Linked Phosphonium Borates. *Chemistry – A European Journal* **2011**, *17* (24), 6731–6743. https://doi.org/https://doi.org/10.1002/chem.201100203.

(81) Stephan, D. W.; W., S. D. The Broadening Reach of Frustrated Lewis Pair Chemistry. *Science (1979)* **2016**, *354* (6317), aaf7229. https://doi.org/10.1126/science.aaf7229.

(82) Stephan, D. W.; Erker, G. Frustrated Lewis Pairs: Metal-Free Hydrogen Activation and More. *Angewandte Chemie International Edition* **2010**, *49* (1), 46–76. https://doi.org/https://doi.org/10.1002/anie.200903708.

(83) Stephan, D. W. Diverse Uses of the Reaction of Frustrated Lewis Pair (FLP) with Hydrogen. *J Am Chem Soc* **2021**, *143* (48), 20002–20014. https://doi.org/10.1021/jacs.1c10845.

(84) Fulmer, G. R.; Miller, A. J. M.; Sherden, N. H.; Gottlieb, H. E.; Nudelman, A.; Stoltz, B. M.; Bercaw, J. E.; Goldberg, K. I. NMR Chemical Shifts of Trace Impurities: Common Laboratory Solvents, Organics, and Gases in Deuterated Solvents Relevant to the Organometallic Chemist. *Organometallics* **2010**, *29* (9), 2176–2179. https://doi.org/10.1021/om100106e.

(85) Bain, G. A.; Berry, J. F. Diamagnetic Corrections and Pascal's Constants. *J Chem Educ* **2008**, *85* (4), 532. https://doi.org/10.1021/ed085p532.

(86) Hill, G. S.; Irwin, M. J.; Levy, C. J.; Rendina, L. M.; Puddephatt, R. J.; Andersen, R. A.; Mclean, L. Platinum(II) Complexes of Dimethyl Sulfide. *Inorganic Syntheses*. January 1, 1998, pp 149–153. https://doi.org/https://doi.org/10.1002/9780470132630.ch25.

(87) Straus, D. A.; Zhang, C.; Tilley, T. D. Trityl Tetraphenylborate as a Reagent in Organometallic Chemistry. *J Organomet Chem* **1989**, *369* (2), C13–C17. https://doi.org/https://doi.org/10.1016/0022-328X(89)88013-1.

Table of contents

This work explores the possibility of tuning the ground state of pyrimidine-bridged Yb-Pt^{IV} heterobimetallic complexes with subtle ligand substitution on the platinum center. This study also allows one to observe the FLP-like behavior of the Pt ion in the presence of a strong Lewis acid and the light-induced reactivity of the tetramethyl-substituted complex.